RESEARCH ARTICLE

3D-Printed Degradable Anti-Tumor Scaffolds for Controllable Drug Delivery

Yucheng Mei[1†], Chengzu He[2†], Chunxia Gao[1], Peizhi Zhu[1*], Guanming Lu[3*], Hongmian Li[4*]

[1]Institute of Biomedical Research and Tissue Engineering, Yangzhou University, Yangzhou 225002, PR China
[2]Department of Oncology, the People's Hospital of Binyang County, Binyang 530405, Guangxi, China
[3]Department of Breast and Thyroid Surgery, Affiliated Hospital of Youjiang Medical University for Nationalities, Baise 533000, Guangxi, China
[4]Research Center of Medical Sciences, The People's Hospital of Guangxi Zhuang Autonomous Region and Guangxi Academy of Medical Sciences, Nanning 530021, China
[†]*These authors contributed equally to this work*

Abstract: In this study, porous polylactic acid/methotrexate (PLA/MTX) scaffolds were successfully fabricated by three-dimensional (3D) printing technology as controllable drug delivery devices to suppress tumor growth. Scanning electron microscopy and energy-dispersive spectrometer confirmed that MTX drug was successfully incorporated into the PLA filament. 3D-printed PLA/MTX scaffolds allow sustained release of drug molecules *in vitro* for more than 30 days, reducing systemic toxic side effects caused by injection or oral administration. *In vitro* cytotoxicity assay revealed that PLA/MTX scaffolds have a relatively high inhibitory effect on the tumor cells (MG-63, A549, MCF-7, and 4T1) and relatively low toxic effect on the normal MC3T3-E1 cells. Furthermore, results of *in vivo* experiments confirmed that PLA/MTX scaffolds highly suppressed tumor growth and no obvious side effects on the organs. All these results suggested that 3D-printed PLA/MTX scaffolds could be used as controllable drug delivery systems for tumor suppression.

Keywords: 3D printing; Polylactic acid; Methotrexate; Anti-tumor

*Correspondence to: Peizhi Zhu, Institute of Biomedical Research and Tissue Engineering, Yangzhou University, Yangzhou 225002, PR China; pzzhu@yzu.edu.cn; Guanming Lu, Department of Breast and Thyroid Surgery, Affiliated Hospital of Youjiang Medical University for Nationalities, Baise 533000, Guangxi, China; luguanming@ymcn.edu.cn; Hongmian Li, Medical Laboratory Center, People's Hospital of Guangxi Zhuang Autonomous Region and Guangxi Academy of Medical Science, Nanning, Guangxi, 530021, China; lihongmian@gxmu.edu.cn

Received: July 20, 2021; **Accepted:** September 1, 2021; **Published Online:** October 1, 2021

Citation: Mei Y, He C, Gao C, *et al*., 2021, 3D-Printed Degradable Anti-Tumor Scaffolds for Controllable Drug Delivery. *Int J Bioprint*, 7(4):418. http://doi.org/10.18063/ijb.v7i4.418

1. Introduction

The mainstream treatment strategy for tumor is to remove the tumor tissue, supplemented by post-operative chemotherapy or radiation therapy. Despite the great progress in treatment for tumor, many adverse post-operative side effects, including the limited distribution of chemotherapy drugs at the target site and severe toxicity after radiotherapy, are unavoidable[1-3]. Therefore, developing a new drug delivery system that can overcome these limitations has become the focus of cancer research.

4-Amino-10-methylfolate (methotrexate [MTX]), an antitumor drug[4], has been widely used to treat various cancer diseases, such as head-and-neck tumors, breast cancer, and lung cancer[5-8]. In spite of its wide application in clinical practice, the treatment with MTX through injection or oral administration is still accompanied by some disadvantages, including non-tissue selectivity, the need for high dose, and high toxicity. In addition, MTX is resistant to bone marrow suppression and gastrointestinal cytotoxicity.

To avoid the shortcomings of injection and oral administration, it is necessary to design a drug delivery system to deliver MTX into the diseased area to achieve the optimal therapeutic effect[9]. Various strategies have been developed to control drug delivery using materials

such as hydrogels, polymer micelles, and stimulus-responsive materials[10-12]. Three-dimensional (3D) printing technology, known as additive manufacturing (AM), has great potential in fabricating the personalized scaffolds[13-15]. Based on the patient's computed tomography (CT) or magnetic resonance imaging (MRI), 3D models can be quickly and accurately established, making it possible to accurately print irregular models[16,17]. Moreover, the drug-loaded scaffolds made by 3D printing technology have unique advantages in personalization, spatial structure, drug components diversity, drug loading accuracy, and drug release sustainability[18-22].

Among various 3D printing technologies, fused deposition modeling (FDM), which was launched by Stratasys in 1992, has become one of the most popular technologies[23]. The technical advantages of FDM include the selectivity of a variety of applicable materials, customized high precision, and low cost[18]. As a typical heat dissipation technology for scaffolding, FDM uses a thermoplastic polymer filament, which is heated to the melting point, and then extruded from the nozzle, and deposited layer by layer to create a scaffold[20,24-27]. The thermoplastic materials used in FDM technology include polylactic acid (PLA), poly(ε-caprolactone) (PCL), poly (methyl methacrylate) (PMMA), polycarbonate (PC), and acrylonitrile butadiene styrene (ABS)[28-35]. Among these thermoplastic materials, PLA has been approved by the FDA as biomedical material due to its excellent biocompatibility[36,37]. Studies demonstrated that 3D printing is a powerful tool for manufacturing personalized scaffolds with specific geometries. Fouladian *et al*. reported that 3D-printed stents loaded with 5-fluorouracil (5-FU) drug were used to treat esophageal cancer. Incorporating anti-cancer drugs into endoluminal stents can provide a sustained release of drugs to esophageal malignant tissues while prolonging the retention of the stent and relieving dysphagia[38].

The purpose of this research is to prepare porous PLA/MTX scaffold with a controllable MTX release. PLA/MTX filaments with different MTX concentrations (MTX mass fraction: 0.5 wt%, 1.5 wt%, and 2.5 wt%) were prepared by melt mixing and extruding method. PLA/MTX scaffolds were printed by FDM using prepared PLA/MTX filament. The morphology, composition, and structure of printed PLA/MTX scaffold were investigated by scanning electron microscopy (SEM) and energy-dispersive spectrometer (EDS). The biocompatibility of printed PLA/MTX scaffolds and the inhibitory effect on tumor cells were evaluated *in vitro* by mouse embryo osteoblast precursor cells (MC3T3-E1), human osteosarcoma cells (MG-63), human breast cancer cells (MCF-7), human lung cancer cell lines (A549), and mouse breast cancer cells (4T1). In addition, the subcutaneous xenograft model was used to explore the inhibitory effect on tumor tissues and the toxicity to normal tissues and organs.

2. Materials and methods

2.1. Materials

PLA (MW: 500 kDa) was purchased from Sigma-Aldrich (Darmstadt, Germany), and MTX was purchased from Bio Basic Inc. (Markham, Ontario, Canada). Cell counting kit-8 (CCK-8) was purchased from Dojindo (Japan). LIVE/DEAD® Viability/Cytotoxicity Kit (Live/Dead) was purchased from Thermo Fisher Scientific (L-3224). The fetal bovine serum (FBS), Dulbecco's Modified Eagle Medium (DMEM), RPMI-1640, penicillin-streptomycin, and trypsin-ethylenediaminetetraacetic acid (EDTA) were purchased from Grand Island (New York, USA). All the reagents were used without further treatment.

2.2. Preparation of the PLA and PLA/MTX composite filaments

The mixture of PLA and MTX was melted and extruded using granulators. PLA/MTX and PLA filament were prepared by the 3D printing consumable extruder (SHSJ, Songhu Machinery Co., Ltd., Dongguan, China) with a 1.75 ± 0.05 mm constant diameter at 220°C and cooled by water, and the screw speed was 45 rpm.

2.3. Fabrication of PLA/MTX scaffolds

The 3D printing bracket was designed using Mimics software and SolidWorks2015 software. STL files were converted to a format (gcode) recognizable by 3D printer (ShanRui DK2, Guangzhou, China) using CURA software. An ink cartridge was added to the 3D printer to transport the PLA/MTX composite filaments, and the filaments were drawn and melted (210°C) and extruded through a nozzle (0.4 mm) to print layer by layer.

2.4. Characterization of PLA/MTX scaffolds

The structures and aperture sizes of PLA/MTX scaffold were characterized using field emission SEM (SEM, Zeiss_Supra55, Germany). Energy-dispersive X-ray analysis (JXA-8230, JEOL, Japan) was then used to perform elemental analysis of the PLA/MTX scaffold surfaces to assess the distribution of MTX in the PLA matrix.

The high-precision digital density meter (ED-1000, Shanghai Tuxin Electronic Technology Co., Ltd.) was used to measure the porosity. The porosity calculation formula is as follows:

$$\text{Porosity } (\%) = (1-(m/\rho)/V) \times 100\%$$

Where, V: outer volume, m: mass, and ρ: density.

2.5. Drug loading capacity and drug release

The 500 mg of PLA/MTX scaffolds were placed in a beaker containing 3 mL $CHCl_3$ to fully dissolve, and then, phosphate-buffered saline (PBS) was used to extract the drug. The absorbance of the PBS was determined by ultraviolet (UV) spectrophotometer at 305 nm.

The 500 mg of scaffold was placed in a 5 mL centrifuge tube containing 3 mL PBS and then shaken at 37°C with a speed of 100 r/min. The absorbance of the scaffolds was determined by UV spectrophotometer at 305 nm and calculated by the following formula.

Loading efficiency % (LE%) = (Weight of encapsulated drug/total mass of the PLA/ MTX scaffold) ×100%

Entrapment efficiency % (EE%) = (Weight of encapsulated drug / Weight of total added drug) × 100%.

2.6. *In vitro* experiments

(1) Cell lines

Mouse embryo osteoblast precursor cells (MC3T3-E1), human osteosarcoma cells (MG-63), human breast cancer cells (MCF-7), human lung cancer cell lines (A549), and mouse breast cancer cells (4T1) were purchased from Shanghai Cell Bank of the Chinese Academy of Sciences (Shanghai, China), and cultured in DMEM (or RPMI) containing 10% FBS and 100 U/mL penicillin-streptomycin.

(2) Cytotoxicity assay

Cells were cultured using 24-well plates with a density of 1×10^4 cells/well. When the cells adhered and spread in plates, the scaffolds were immersed into the culture medium. The CCK-8 assay was performed on days 1, 3, and 5. Briefly, the culture medium of the sample was replaced with 100 μL DMEM (RPMI) and incubated at 37°C for 2.5 h. The absorbance was measured at 450 nm in the Multiskan FC enzyme labeling instrument (Thermo, Waltham, USA). The cell viability was evaluated by live/dead staining. After incubation in the medium for 12 h, 24 h, 72 h, and 120 h, 4 μM Calcein-AM and 2 μM ethidium homodimer-1 were added to stain living cells and dead cells, respectively. After incubated at 37°C for 15 min, the cells were examined using fluorescence microscope (Olympusix53, Tokyo, Japan).

2.7. *In vivo* anti-tumor effect

(1) Subcutaneous xenograft model

The 4T1 cells (2×10^5) were subcutaneously injected into the back of the BALB/c mice to establish the subcutaneous xenograft model. After surgery, celecoxib (Dalian Meilun Biotechnology, China) was given to relieve postoperative pain (10 mg/kg, gavage, q.d./2 days) and ceftriaxone sodium (Dalian Meilun Biotechnology, China) to prevent post-operative infection (20 mg/kg, tail vein injection, q.d./2 days). The mice were housed under the standard conditions.

(2) In vivo antitumor efficacy and mechanism studies

When tumor volume reached approximately 62.50 ± 10 mm^3 (5 mm×5 mm×5 mm), mice bearing 4T1 tumors were randomly assigned to four groups with five mice in each group. The injection group was administered an intraperitoneal injection of drugs every 2 days of MTX at 4 mg/kg. The PLA/MTX scaffolds printed from filament were implanted near the tumors. The tumor size and the weight of mice were recorded every day. The animals were euthanized at the end point (21 days), and the major organs (heart, liver, spleen, lung, and kidney) were collected for weighing to calculate organ coefficient and then fixed in 4% paraformaldehyde for histopathological examination. The animal research was approved by the Experimental Animal Ethics Committee of Yangzhou University (NSFC2020-HXXY-4).

2.8. Statistical analysis

All the experiments were performed in triplicate. Results were expressed as mean ± standard deviation (SD). Bonferroni post-test was performed to assess statistical significance. Statistical analysis was performed using non-parametric Kruskal–Wallis tests. $P < 0.05$ was considered statistically significant.

3. Results

3.1. Morphological, composition, and structural analysis

The morphology, microstructure, and compositions were investigated by SEM and EDS (**Figure 1**). According to **Figure 1A-1**, SEM image of the PLA/MTX scaffold showed a relatively smooth surface and had open big pores in uniform size with integrated lines (755 ± 0.7 μm) among the big pores. Moreover, the printed PLA/MTX scaffolds were porous, with the porosity and pore size at 29.7% and 309 ± 0.5 μm, respectively.

The EDS spectra are shown in **Figure 1B**, and the peaks of C, N, and O were observed in the spectrum of PLA/MTX scaffold. The appearance of N peak confirmed that MTX was introduced into PLA matrix. The color map obtained from EDS analysis in **Figure 1A** shows the N (blue) distribution in the scaffold structure, which proves that MTX was well distributed in the PLA matrix. The evenly dispersion of MTX in the scaffold provides the possibility for MTX to be released along with PLA degradation.

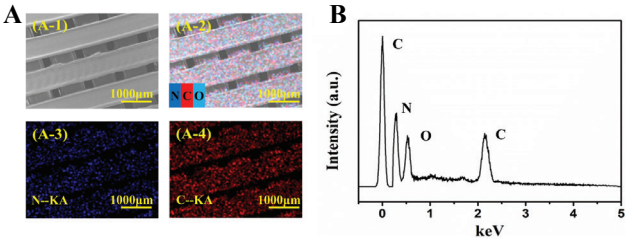

Figure 1. The morphology, composition, and structure of printed polylactic acid/methotrexate (PLA/MTX) and PLA scaffolds. (A) Scanning electron microscopy images of PLA/MTX scaffolds. Scale bars represent 1 mm for A. Element mapping of C, N, and O for the PLA/MTX scaffold. Scale bars represent 1 mm. (B) Energy-dispersive spectrometer of porous printed PLA/MTX composite scaffolds.

3.2. Characterization of drug loading (LE%) and encapsulation efficiency (EE%) in PLA/MTX scaffolds and drug release profiles *in vitro*

Before assessing the release profiles of MTX from PLA/MTX scaffolds with different drug concentrations, the LE% and EE% were calculated by measuring the concentration of drug absorbance in the PBS. The EE% of MTX was 98.1% and the LE% of MTX was controlled at 0.5%, 1.5%, and 2.5%.

The release profiles of MTX from PLA/MTX scaffolds are shown in **Figure 2**. Approximately 25% of MTX was released within the first 24 h, and about 50% of MTX was released within the first 7 days. 3D-printed PLA/MTX scaffolds allow sustained release of drugs *in vitro* more than 30 days. In addition, with the increase of drug content, the release trend of MTX is basically similar. Therefore, the drug release could be controlled by adjusting MTX content in scaffolds. This result proved that PLA/MTX scaffolds had a sustained release effect.

Figure 3 shows the comparison of MTX release profiles of 3D-printed PLA/MTX scaffolds of varying drug contents and cast PLA/MTX with 0.5% of MTX over 5 days. The drug release pattern of cast PLA/MTX sample is similar to that of 3D-printed porous PLA/MTX scaffold. However, the drug release rate of the cast PLA/MTX sample is slower than that of 3D-printed PLA/MTX scaffold. In cast PLA/MTX sample, the MTX drug molecules were wrapped tightly by PLA material to obstruct the release of drug molecules from the polymer matrix. The release of MTX from 3D-printed porous PLA/MTX scaffold is more stable than cast sample.

3.3. In vitro cytotoxicity

Figure 4 shows the *in vitro* inhibitory effect of PLA/MTX scaffolds on human lung cancer cell lines (A549), human osteosarcoma cells (MG-63), human breast cancer cells (MCF-7), and normal mouse embryo

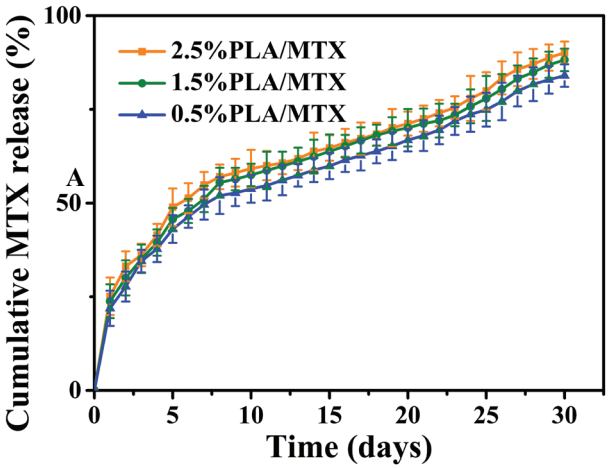

Figure 2. Methotrexate (MTX) release profiles of polylactic acid/MTX (PLA/MTX) scaffolds of varying drug content over 7 and 30 days.

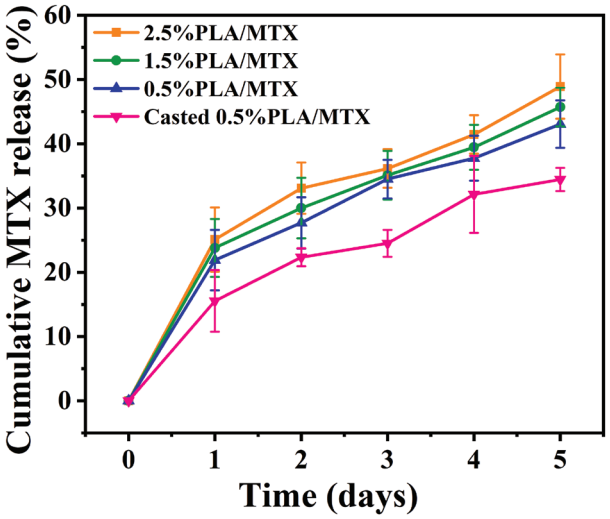

Figure 3. Methotrexate (MTX) release profiles of polylactic acid/MTX (PLA/MTX) scaffolds of varying drug contents and cast PLA/MTX with 0.5% of MTX over 5 days.

osteoblast precursor cells (MC3T3-E1). As shown in **Figure 4A-C**, the inhibitory effect increases as the drug content increases. The growth of tumor cells (A549, MG-63, and MCF-7) has been significantly inhibited at 24 h. At the same time, the inhibitory effect increased as the administration time was extended to the third and 5th days. Each PLA/MTX scaffold has a 95% inhibition rate of tumor cells at the 120 h. The above results indicate that the implantable PLA/MTX scaffold showed strong anti-tumor efficacy compared with PLA group and control group. The toxicity of PLA and PLA/MTX scaffolds on normal MC3T3 cells was also investigated (**Figure 4D**). The results showed that PLA scaffold had little effect on the growth of normal cells,

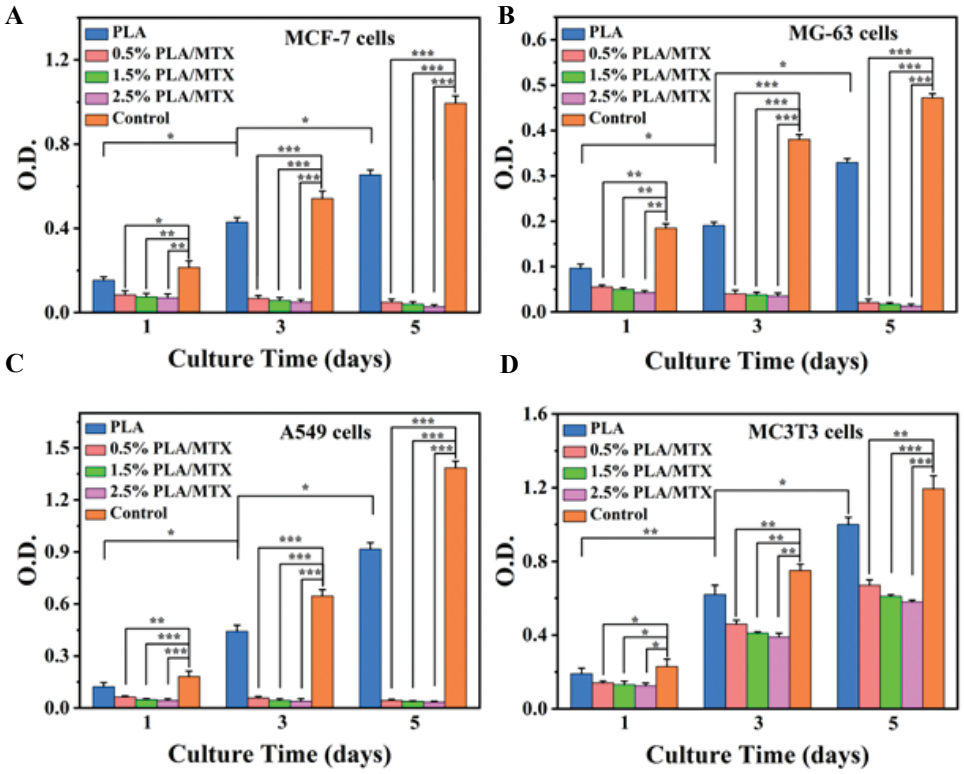

Figure 4. Evaluation of anticancer effect *in vitro*. *In vitro* proliferation of MCF-7(A), MG- 63 (B), A549 (C), and MC3T3 (D) cells after culturing in the polylactic acid/methotrexate (0.5%, 1.5%, and 2.5%) scaffolds and the tissue culture plate substrate (as control) for 1, 3, and 5 days.

while PLA/MTX scaffold had some effect on normal cells, but the effect was limited.

As shown in **Figure 5**, the toxicity of PLA and PLA/MTX scaffolds on cancer cells was also investigated by Live/Dead fluorescence staining of mouse breast cancer 4T1 cells. Due to its excellent biocompatibility, PLA scaffold group has low cytotoxicity within 120 h. The PLA/MTX scaffold groups showed a lower cell survival rate compared with PLA group and control group, and the inhibitory effect increased with the prolonged culture time. With the gradual release of MTX from the scaffold, the cell viability in the PLA/MTX scaffold group decreased. With the increase of drug concentration and culture time, the number of living cells gradually decreased and the number of dead cells gradually increased. The total induction of apoptosis of 4T1 cells by PLA/MTX scaffolds increased from 52.89% to 99.63% (**Figure 4C**). Thus, compared with the PLA and control groups, the PLA/MTX scaffolds showed strong inhibitory effect on tumor 4T1 cells.

3.4. *In vivo* anti-tumor effect

As shown in **Figure 6**, the anti-tumor effects of PLA/MTX scaffolds were evaluated by subcutaneous xenograft model of 4T1 tumor-bearing Balb/c mice compared with intraperitoneal drug injection of MTX. The minor body weight changes in implant groups (**Figure 6A**) proved that the implanted scaffolds were well tolerated by the mice. Weight loss occurred in the 0.5% PLA/MTX and 2.5% PLA/MTX groups at the beginning due to surgical anesthesia, surgical implantation, and other operations, but the growth status in the middle and later stages was the same as the control group (**Figure 6A**). Throughout the experiment, the overall growth of mice in the negative control group was good, but one mouse in the control group was paralyzed due to excessive compression of the spine by the tumor. In the early stage, the growth state of the injection group was the same as that of the control group. In the later stage, there were some adverse phenomena, such as weight loss, bad hair, small and sticky stool, and scorched yellow urine. There was no significant difference in organ coefficient of heart, liver, lung, and kidney among groups. The organ coefficient of spleen in injection group was much lower than the other three groups, which was found at the time of dissection (**Figure 6B**). The tumor sizes in **Figure 6C** can directly show that PLA/MTX scaffold implantation significantly inhibited the tumor growth compared with control group. The anti-tumor effects of 0.5% PLA/MTX scaffold with low concentration of drug are similar to

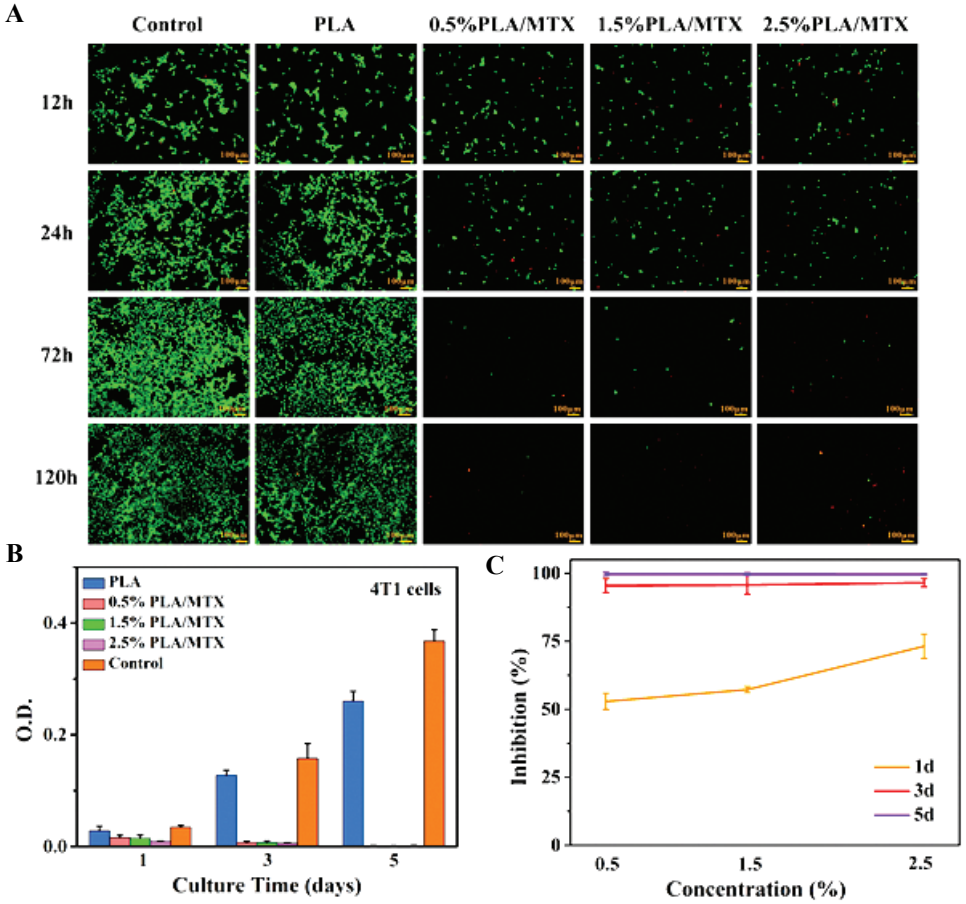

Figure 5. Evaluation of anticancer effect *in vitro*. (A) Live/Dead fluoresce staining of 4T1 cells on polylactic acid/methotrexate (PLA/MTX). The cells were cultured in DMEM for 12 h, 24 h, 72 h, and 120 h. Viable cells are stained green while dead cells red. (B) *In vitro* proliferation of 4T1 cells after culturing in the PLA/MTX (0.5%, 1.5%, and 2.5%) scaffolds and the tissue culture plates substrate (as control) for 1, 3, and 5 days. (C) Inhibition rate at different MTX concentrations.

that of injection group. The anti-tumor effects of 2.5% PLA/MTX scaffold with high concentration of drug were relatively better than that of 0.5% PLA/MTX scaffold with low concentration of drug (**Figure 6D**). The mean tumor volume of the control group was above 1300 mm^3, which was much larger than tumor volume in the 0.5% PLA/MTX and 2.5% PLA/MTX groups (<400 mm^3).

As shown in **Table 1**, PLA/MTX scaffold groups were more effective than the MTX injection in controlling tumor growth. The anti-tumor effect of the 2.5% PLA/MTX scaffold group was also significantly different from that of the 0.5% PLA/MTX group ($P < 0.05$). The main reason is that the injected drug is eliminated by renal metabolism in a short time, resulting in a short plasma half-life (5-8 h) and low drug concentration in target tissues. The tumor growth inhibition value (TGI) of high concentration group could reach 89.26%, which was higher than 74.04% in injection group. The results indicated that PLA/MTX scaffold had a better therapeutic effect than the intraperitoneal injection of drugs.

Table 1. Tumor weight and tumor growth inhibition value (TGI) of each group

Group	Tumor weight (g)	TGI
2.5% PLA/MTX	0.1557±0.024	89.26%
0.5% PLA/MTX	0.33524±0.042	76.88%
Injection	0.3763±0.018	74.04%
Control	1.45±0.3	-

TGI, tumor growth inhibition value.

The hematoxylin and eosin (H and E) staining results in **Figure 7** showed that some area of tumor necrosis appeared in the sections of 0.5% PLA/MTX group, 2.5% PLA/MTX group, and injection group. The nuclei of cancer cells enlarged, produced cavities and the cells showed apoptosis and necrosis. Eventually, the nucleus breaks, creating a "ghost" area. There was no obvious tumor necrosis in the control group. No obvious metastasis and inflammatory were found in the 0.5% PLA/MTX group and 2.5% PLA/MTX group, while the control group showed metastases. The H and E staining

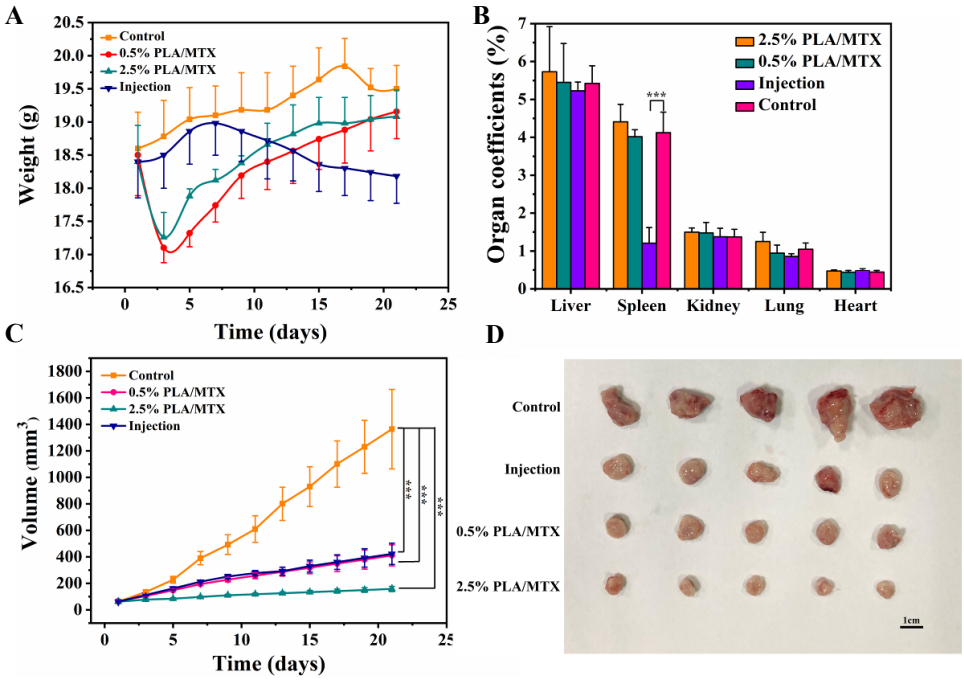

Figure 6. Evaluation of therapeutic efficiency of scaffolds *in vivo*. (A) Time-dependent body weight of the mice after different treatments. (B) Organ coefficients. (C) Time-dependent tumor growth curves of the mice with different treatments. (D) Photographs of the harvested tumors on day 21 from mice with different treatments.

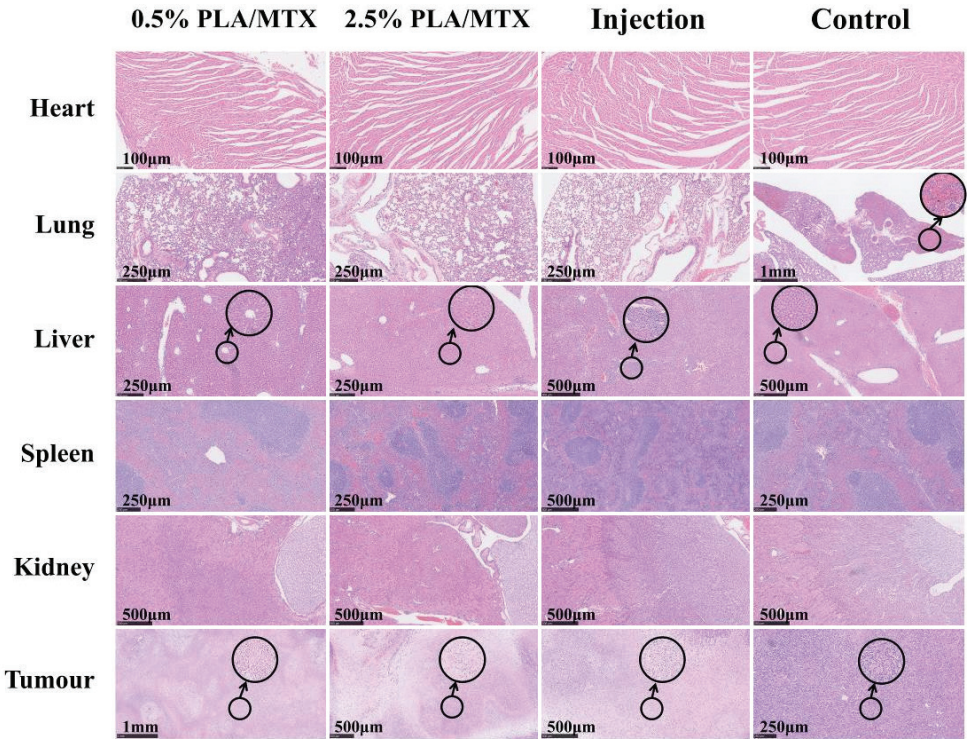

Figure 7. H &E staining results of experimental endpoint. The representative H and E staining images of the tumor, heart, liver, spleen, lung, and kidney from Balb/c mice with indicated treatment. Explanation about the circled area: In the tumor slices of 0.5% polylactic acid/methotrexate (PLA/MTX), 2.5% PLA/MTX, and injection group, the circled area indicates that tumor necrosis occurred in some areas, forming a "ghost" area. In the control group, the structure of tumor cells in the circled area was stable, the nuclei were clearly visible and arranged regularly. In the control group, metastases and increased inflammatory cells appeared in the circled area of lung sections. There were more inflammatory cells (lymphocytes, leukocytes and monocytes, etc.) in the liver slices of injection group. Scale bars represent 100, 250, 500, and 1000 μm.

of the spleen showed that the injection group had obvious white hyperplasia and more inflammatory cells (B-cell monocytes, etc.). There was no obvious nephrotoxicity found in all four groups.

4. Discussion

As shown in **Figure 8**, under the guidance of computer-aided design (CAD) and 3D printing technology, PLA/MTX drug-loaded scaffold was prepared by FDM printer. Then, PLA/MTX drug-loaded scaffold was implanted into the mouse body. With the release of MTX, the growth and reproduction of tumor cells were inhibited. The drug release from the PLA/MTX scaffold showed a sustained and slow process due to the degradation process of PLA[39]. The CCK-8 assay demonstrated that the PLA material did not exert severe cytotoxic effects on 4T1, A549, MCF-7, MG-63, and MC3T3 cells. *In vitro* cellular experiments revealed that the printed PLA/MTX scaffolds have a relatively high inhibitory effect on the tumor cells MG-63, A549, MCF-7, and 4T1, and lower toxic effect on the normal cells MC3T3-E1. The inhibition rates of three different concentrations of PLA/MTX scaffolds on cancer cells were more than 95% after cultured for 5 days.

After 3 weeks of observation, PLA/MTX scaffold with different MTX concentrations group had a higher tumor inhibition rate. We found that PLA/MTX scaffold was better than MTX injection in controlling tumor growth. This was attributed to an enrichment of the released MTX around the tumor tissue and lasting therapeutic MTX levels for prolonged time. The intraperitoneal delivery of MTX needed injection of drug every 2 days while PLA/MTX scaffold was implanted only once for the treatment, indicating that the PLA/MTX drug delivery system was more efficient than traditional injection method.

In a word, 3D-printed PLA/MTX scaffolds maintained a high tumor inhibition rate and significantly reduced systemic drug toxicity compared with intraperitoneal injection. The implanted PLA/MTX scaffolds can release and maintain therapeutic drug levels at the tumor site for prolonged time while reducing systemic drug exposure to healthy tissues. Moreover, this implantable scaffold only requires 1 time implantation, which greatly reduces the frequency of drug administration. Therefore, PLA/MTX scaffold as a controllable drug delivery system has great potential for suppressing tumor growth.

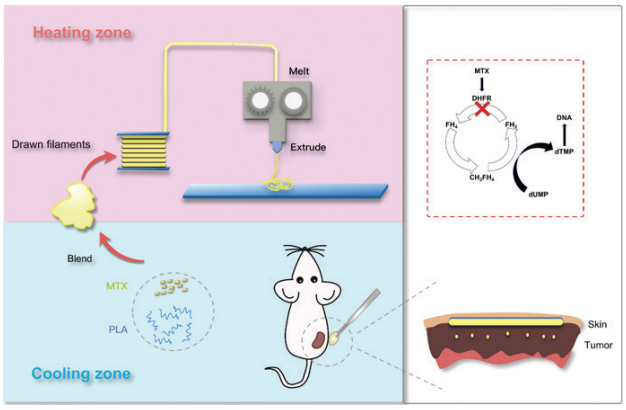

Figure 8. Schematic illustration of the fabrication and application of PLA/methotrexate scaffolds for tumor therapy.

5. Conclusions

We developed a novel 3D-printed drug delivery scaffold for tumor therapy. Morphological and structural analysis results showed that MTX was successfully incorporated into the PLA filament. PLA/MTX scaffolds can maintain MTX release for more than 30 days. *In vitro* cytotoxicity experiments confirmed that PLA/MTX scaffolds have a relatively high inhibitory effect on tumor cells while showing less toxicity to normal cells. In addition, *in vivo* results demonstrated that the PLA/MTX scaffolds highly suppressed tumor growth with negligible side effects on the normal tissues and organs. 3D-printed PLA/MTX scaffolds could be used as a controllable drug delivery system and have the great potential for suppressing tumor growth.

Funding

This research was supported by Technology Department of Yangzhou City (YZ2019073) from Jiangsu Huadong Medical Device Industrial Co., Ltd., China. A project funded by the Priority Academic Program Development of Jiangsu Higher Education Institutions, Guangxi Natural Science Foundation (2019JJA140071), and the First Batch of High-level Talent Scientific Research Projects of the Affiliated Hospital of Youjiang Medical University for Nationalities in 2019 (Contract No. R20196307).

Conflicts of interest

The authors declare that they have no conflicts of interest.

Authors' contributions

P.Z., C.H., and Y.M. conceived the project. Y.M. and C.H. conducted the scaffold fabrication and characterization. C.H. and C.G. conducted the cell and animal study. P.Z. reviewed the experimental results and advised the organization of the main contents. P.Z., G.L., H.L, C.G., and Y.M. wrote the manuscript.

References

1. O'Reilly M, Mellotte G, Ryan B, 2020, Gastrointestinal Side Effects of Cancer Treatments. *Ther Adv Chronic Dis*, 11:1-7. https://doi.org/10.1177/2040622320970354
2. Nandini D B, Rao R S, Hosmani J, *et al*., 2020, Novel

Therapies in the Management of Oral Cancer: An Update. *Dis Mon*, 66:101036.
https://doi.org/10.1016/j.disamonth.2020.101036

3. van Kaick G, Delorme S, 2008, Therapy-Induced Effects in Normal Tissue. *Radiologe*, 48:871–80.
https://doi.org/10.1007/s00117-008-1729-3
4. Fiehn C, 2011, The Future of Methotrexate Therapy and Other Folate Inhibitors. *Z Rheumatol*, 70:129–34.
https://doi.org/10.1007/s00393-010-0688-z
5. Sparano JA, Gray RJ, Makower, D, *et al*., 2020, Clinical Outcomes in Early Breast Cancer With a High 21-Gene Recurrence Score of 26 to 100 Assigned to Adjuvant Chemotherapy Plus Endocrine Therapy: A Secondary Analysis of the TAILORx Randomized Clinical Trial. *JAMA Oncol*, 6:367–74.
https://doi.org/10.1001/jamaoncol.2019.4794
6. Cohen EE, Soulieres D, Le Tourneau C, 2019, Pembrolizumab Versus Methotrexate, Docetaxel, or Cetuximab for Recurrent or Metastatic Head-and-Neck Squamous Cell Carcinoma (KEYNOTE-040): A Randomised, Open-Label, Phase 3 Study. *Lancet*, 393:156–67.
https://doi.org/10.1016/S0140-6736(18)31999-8
7. Bielack SS, Smeland S, Whelan JS, *et al*., 2015, Methotrexate, Doxorubicin, and Cisplatin (MAP) Plus Maintenance Pegylated Interferon Alfa-2b Versus MAP Alone in Patients With Resectable High-Grade Osteosarcoma and Good Histologic Response to Preoperative MAP: First Results of the EURAMOS-1 Good Response Randomized Controlled Trial. *J Clin Oncol*, 33:2279–87.
https://doi.org/10.1200/JCO.2014.60.0734
8. Suksiriworapong J, Taresco V, Ivanov DP, *et al*., 2018, Synthesis and Properties of a Biodegradable Polymer-Drug Conjugate: Methotrexate-Poly(Glycerol Adipate). *Colloids Surf B Biointerfaces*, 167:115–25.
https://doi.org/10.1016/j.colsurfb.2018.03.048
9. Zhong SH, Liu P, Ding JS, *et al*., 2021, Hyaluronic Acid-Coated MTX-PEI Nanoparticles for Targeted Rheumatoid Arthritis Therapy. *Crystals*, 11:321.
https://doi.org/10.3390/cryst11040321
10. Ghobashy MM, Elbarbary AM, Hegazy DE, 2021, Gamma Radiation Synthesis of a Novel Amphiphilic Terpolymer Hydrogel pH-Responsive Based Chitosan for Colon Cancer Drug Delivery. *Carbohydr Polym*, 263:117975.
https://doi.org/10.1016/j.carbpol.2021.117975
11. Fu YP, Ding Y, Zhang LT, *et al*., 2021, Poly Ethylene Glycol (PEG)-Related Controllable And Sustainable Antidiabetic Drug Delivery Systems. *Eur J Med Chem*, 217:113372.
https://doi.org/10.1016/j.ejmech.2021.113372
12. Song FY, Gong JW, Tao YH, *et al*., 2021, A Robust Regenerated Cellulose-Based Dual Stimuli-Responsive Hydrogel as an Intelligent Switch for Controlled Drug Delivery. *Int J Biol Macromol*, 176:448–58.
https://doi.org/10.1016/j.ijbiomac.2021.02.104
13. Koons GL, Diba M, Mikos AG, 2020, Materials Design for Bone-Tissue Engineering. *Nat Rev Mater*, 5:584–603.
14. Lepowsky E, Tasoglu S, 2018, 3D Printing for Drug Manufacturing: A Perspective on the Future of Pharmaceuticals. *Int J Bioprint*, 4:119.
https://doi.org/10.18063/IJB.v4i1.119
15. Jimenez M, Romero L, Dominguez I A, *et al*., 2019, Additive Manufacturing Technologies: An Overview about 3D Printing Methods and Future Prospects. *Complexity*, 2019:9656938.
https://doi.org/10.1155/2019/9656938
16. Bozo II, Deev RV, Smirnov IV, *et al*., 2020, 3D Printed Gene-activated Octacalcium Phosphate Implants for Large Bone Defects Engineering. *Int J Bioprint*, 6:275.
https://doi.org/10.18063/ijb.v6i3.275
17. Gatenholm B, Lindahl C, Brittberg M, *et al*., 2020, Collagen 2A Type B Induction after 3D Bioprinting Chondrocytes *In Situ* into Osteoarthritic Chondral Tibial Lesion. *Cartilage*, 2020:1-15.
https://doi.org/10.1177/1947603520903788
18. Zhang B, Cristescu R, Chrisey DB, *et al*., 2020, Solvent-based Extrusion 3D Printing for the Fabrication of Tissue Engineering Scaffolds. *Int J Bioprint*, 6:211.
https://doi.org/10.18063/ijb.v6i1.211
19. Wang H, Vijayavenkataraman S, Wu Y, *et al*., 2021, Investigation of process Parameters of Electrohydro-Dynamic Jetting for 3D Printed PCL Fibrous Scaffolds with Complex Geometries. *Int J Bioprint*, 2:63–71.
20. An J, Teoh JE, Suntornnond R, *et al*., 2015, Design and 3D Printing of Scaffolds and Tissues. *Engineering*, 1:261–8.
21. Long JJ, Gholizadeh H, Lu J, *et al*., 2017, Application of Fused Deposition Modelling (FDM) Method of 3D Printing in Drug Delivery, *Curr Pharm Des*, 23:433–9.
22. Tappa K, Jammalamadaka U, 2018, Novel Biomaterials Used in Medical 3D Printing Techniques. *J Funct Biomater*, 9:17.
https://doi.org/10.3390/jfb9010017
23. Daminabo SC, Goel S, Grammatikos SA, *et al*., 2020, Fused Deposition Modeling-Based Additive Manufacturing (3D Printing): Techniques for Polymer Material Systems. *Mater Today Chem*, 16:100248.
https://doi.org/10.1016/j.mtchem.2020.100248
24. Ranjan N, Singh R, Ahuja IP, *et al*., 2020, On 3D Printed

Scaffolds for Orthopedic Tissue Engineering Applications. *SN Appl Sci*, 2:192.

25. Nurulhuda A, Aqmaliah SH, Ali R, *et al*., 2019, Multi-Layered ABS Scaffold Fabrication via Fused Deposition Modelling (FDM) 3D Printing. *J Mech Contin Math Sci*, 4:131–8. https://doi.org/10.26782/jmcms.spl.4/2019.11.00013
26. Wang ZZ, Yang Y, 2021, Application of 3D Printing in Implantable Medical Devices. *Biomed Res Int*, 2021:6653967. https://doi.org/10.1155/*2021*/6653967
27. Limongi T, Susa F, Allione M, *et al*., 2020, Drug Delivery Applications of Three-Dimensional Printed (3DP) Mesoporous Scaffolds. *Pharmaceutics*, 12:851. https://doi.org/10.3390/pharmaceutics12090851
28. Zhang B, Seong B, Nguyen V, *et al*., 2016, 3D Printing of High-Resolution PLA-Based Structures by Hybrid Electrohydrodynamic and Fused Deposition Modeling Techniques. *J Micromech Microeng*, 26:025015. https://doi.org/10.1088/0960-1317/26/2/025015
29. Hedayati SK, Behravesh AH, Hasannia S, *et al*., 2020, 3D Printed PCL Scaffold Reinforced with Continuous Biodegradable Fiber Yarn: A Study on Mechanical and Cell Viability Properties. *Polym Test*, 83:106347.
30. Babu NV, Venkateshwaran N, Rajini N, *et al*., 2021, Influence of Slicing Parameters on Surface Quality and Mechanical Properties of 3D-Printed CF/PLA Composites Fabricated by FDM teChnique. *Mater Technol*, 2021:1-18. https://doi.org/10.1080/10667857.2021.1915056
31. Viidik L, Vesala J, Laitinen R, *et al*., 2021, Preparation and Characterization of Hot-Melt Extruded Polycaprolactone-Based Filaments Intended for 3D-Printing of Tablets. *Eur J Pharm Sci*, 158:105619.
32. Solorio-Rodriguez LE, Vega-Rios A, 2019, Filament Extrusion and Its 3D Printing of Poly(Lactic Acid)/ Poly(Styrene-co-Methyl Methacrylate) Blends. *Appl Sci*, 9:5153.
33. Chen PC, Chou CC, Chiang CH, Systematically Studying Dissolution Process of 3D Printed Acrylonitrile Butadiene Styrene (ABS) Mold for Creation of Complex and Fully Transparent Polydimethylsiloxane (PDMS) Fluidic Devices. *BioChip J*, 15:144–51.
34. Andrzejewski J, Marciniak-Podsadna L, 2020, Development of Thermal Resistant FDM Printed Blends. The Preparation of GPET/PC Blends and Evaluation of Material Performance. *Materials*, 13:2057. https://doi.org/10.3390/ma13092057
35. Baran EH, Erbil HY, 2019, Surface Modification of 3D Printed PLA Objects by Fused Deposition Modeling: A Review. *Colloid Interface*, 3:43. https://doi.org/10.3390/colloids3020043
36. Singhvi MS, Zinjarde SS, Gokhale DV, 2019, Polylactic Acid: Synthesis and Biomedical Applications. *J Appl Microbiol*, 127:1612–26. https://doi.org/10.1111/jam.14290
37. Lasprilla AJ, Martinez GA, Lunelli BH, *et al*., 2012, Poly-Lactic Acid Synthesis for Application in Biomedical Devices-a Review. *Biotechnol Adv*, 30:321–8. https://doi.org/10.1016/j.biotechadv.2011.06.019
38. Fouladian P, Kohlhagen J, Arafat M, *et al*., 2020, Three-Dimensional Printed 5-Fluorouracil Eluting Polyurethane Stents for the Treatment of Oesophageal Cancers. *Biomater Sci*, 8:6625–36. https://doi.org/10.1039/d0bm01355b
39. Gorrasi G, Pantani R, 2018, Hydrolysis and Biodegradation of Poly (Lactic Acid). *Adv Polym Sci*, 279:119–51.